Acta Crystallographica Section D
Biological Crystallography
ISSN 0907-4449

Structure of *Rhodoferax fermentans* high-potential iron–sulfur protein solved by MAD

Ana González,[a] Stefano Benini[b] and Stefano Ciurli[c]*

[a]Stanford Synchrotron Radiation Laboratory, 2575 Sand Hill Road MS99, Menlo Park, CA 94025, USA, [b]York Structural Biology Laboratory, Department of Chemistry, University of York, Heslington, York YO10 5YW, England, and [c]Department of Agro-Environmental Science and Technology, University of Bologna, Viale Fanin 40, I-40100 Bologna, Italy

Correspondence e-mail: stefano.ciurli@unibo.it

Received 7 May 2003
Accepted 30 June 2003

PDB Reference: *R. fermentans* HiPIP, 1hlq, r1hlqsf.

The crystal structure of *Rhodoferax fermentans* high-potential iron protein (HiPIP) has been solved by MAD methods using the anomalous signal from the Fe atoms in the $[Fe_4S_4]$ cluster present in the protein and refined to a resolution of 1.45 Å. The peptide chain is well defined except in the N- and C-terminal areas. The structure of the protein reveals the presence of three helical fragments, a small β-sheet and several turns, with the $[Fe_4S_4]$ cluster being located close to a surface patch containing several well conserved aromatic residues. The protein fold is very similar to the structures of other known HiPIPs, especially in the region proximal to the $[Fe_4S_4]$ cluster, while the largest differences are observed on the opposite side of the protein, which is rich in positive charges and has no sequential homology to other HiPIP families.

1. Introduction

HiPIPs (high-potential iron–sulfur proteins) are a class of small (8–10 kDa) proteins containing a cubane $[Fe_4S_4]$ cluster bound to the protein backbone by four Fe–S Cys bonds (Carter, 2001). HiPIPs are peculiar among iron–sulfur proteins because of the high reduction potential at which the metal cluster exchanges electrons (from +50 to +450 mV; Meyer *et al.*, 1983) using the $[Fe_4S_4]^{3+/2+}$ couple (Carter *et al.*, 1972; Middleton *et al.*, 1980). HiPIPs have been extensively investigated as electron-transfer models (Rawlings *et al.*, 1976; Mizrahi *et al.*, 1976, 1980; Mizrahi & Cusanovich, 1980; Aprahamian & Feinberg, 1981; Meyer *et al.*, 1983, 1995; Przysiecki *et al.*, 1985; Babini *et al.*, 2000) and their electronic, spectroscopic and redox properties are well characterized (Bertini *et al.*, 1995; Capozzi *et al.*, 1998). Even though the structures of several HiPIPs have been determined (Carter *et al.*, 1974; Freer *et al.*, 1975; Breiter *et al.*, 1991; Rayment *et al.*, 1992; Benning *et al.*, 1994; Kerfeld *et al.*, 1998; Parisini *et al.*, 1999; Nogi *et al.*, 2000, Liu *et al.*, 2002), their biological function is still a matter of discussion.

HiPIPs were initially shown to participate in direct (Hooper & Di Spirito, 1985) and indirect (Tedro *et al.*, 1977; Fukumori & Yamanaka, 1979; Kusano *et al.*, 1992) substrate-oxidation reactions in purple sulfur bacteria. In recent years, attention has been directed towards the involvement of HiPIPs in the respiratory (Bonora *et al.*, 1999) or photosynthetic machinery of phototrophic bacteria. This possibility is supported by the fact that HiPIPs are abundant in most species of purple phototrophic bacteria that lack cytochrome c_2 (Bartsch, 1991). The latter are well established electron carriers in the cyclic

Table 1
Data processing and merging statistics.

Values in parentheses are for the last resolution bin.

λ (Å)	0.995	1.742	1.738	1.105
Resolution (Å)	29.488–2.140 (2.26–2.14)	29.428–2.408 (2.56–2.41)	25.410–2.371 (2.39–2.37)	22.086–1.452 (1.53–1.45)
No. of reflections†	61057 [60157]	54043 [53913]	45443 [45077]	239390 [238478]
No. of unique reflections†	13425 [12525]	9678 [9548]	10102 [9736]	42770 [41858]
R_{sym}	0.046 (0.138)	0.071 (0.284)	0.081 (0.304)	0.047 (0.412)
R_{anom}	0.035 (0.094)	0.050 (0.166)	0.079 (0.259)	0.038 (0.293)
$I/\sigma(I)$	12.6 (5.3)	9.9 (2.6)	8.8 (2.4)	6.9 (0.6)
Completeness (%)	97.4 (91.4)	98.1 (89.4)	98.2 (53.1)	99.0 (95.4)
Multiplicity	4.5 (4.4)	5.6 (5.1)	4.5 (2.1)	5.6 (3.8)
Anomalous completeness (%)	93.4 (89.9)	99.0 (93.8)	98.1 (51.4)	99.1 (95.7)

† Values in square brackets indicate the number of reflections with more than one measurement.

photosynthetic electron flow, able to shuttle electrons between the membrane-bound complexes cytochrome bc_1 (the reductant) (Prince *et al.*, 1978) and the photosynthetic reaction centre (RC) (the oxidant) (Prince *et al.*, 1974; Dutton & Leigh, 1975; Bowyer *et al.*, 1979; Overfield *et al.*, 1979; Okamura & Feher, 1983; Shill & Wood, 1984; Moser & Dutton, 1988; Knaff *et al.*, 1991; Meyer *et al.*, 1993; Tiede *et al.*, 1993; Venturoli *et al.*, 1993; Lin *et al.*, 1994). Therefore, a role for HiPIPs as alternative electron carriers was proposed (Bartsch, 1991; Meyer & Donohue, 1995), but has only recently been well established.

A study performed on membranes isolated from *Rhodoferax* (*Rf.*) *fermentans*, a non-sulfur purple facultative phototrophic bacterium (Hiraishi *et al.*, 1991) lacking cytochrome c_2 (Hochkoeppler, Moschettini *et al.*, 1995; Hochkoeppler, Zannoni *et al.*, 1995) but expressing large amounts of HiPIP (Hochkoeppler, Kofod *et al.*, 1995), provided the very first direct evidence for the physiologically compatible kinetics of HiPIP photo-oxidation (Hochkoeppler, Ciurli *et al.*, 1995). Subsequently, analogous evidence was suggested by studies performed in whole cells or in membrane suspensions of *Rubrivivax* (*Ru.*) *gelatinosus* (Schoepp *et al.*, 1995; Osyczka *et al.*, 1997, 1998; Osyczka, Nagashima, Shimada *et al.*, 1999; Osyczka, Nagashima, Sogabe *et al.*, 1999) and *Rhodocyclus* (*Rh.*) *tenuis* (Menin *et al.*, 1997), as well as *Ectothiorhodospira vacuolata*, *Chromatium vinosum*, *C. purpuratum* and *Rhodopila* (*R.*) *globiformis* (Menin *et al.*, 1998). A detailed investigation of the kinetics of electron transfer between isolated HiPIP and RC from *Rf. fermentans* was reported in 1996 (Hochkoeppler *et al.*, 1996). This study demonstrated the very fast ($t_{1/2}$ = 2.2 µs) rate of re-reduction of the highest potential heme c_{556}, which belongs to the RC tetraheme subunit, by the HiPIP from the same bacterial species. Such a high intrinsic value of the electron-transfer rate, still unmatched in the case of experiments involving membrane suspensions or whole cells, strongly supported a physiological role for HiPIP in photocyclic electron transfer (Hochkoeppler *et al.*, 1996).

Rf. fermentans HiPIP, a 75-amino-acid protein, has been characterized by means of a variety of spectroscopic techniques (Hochkoeppler, Kofod *et al.*, 1995; Ciurli *et al.*, 1996) and its sequence has been determined (Van Driessche *et al.*, 1997). Here, we report the crystal structure of this protein and carry out a comparison with other HiPIPs that have been structurally characterized to date.

2. Materials and methods

2.1. Protein crystallization

Rf. fermentans HiPIP was purified as previously described (Hochkoeppler, Kofod *et al.*, 1995). The protein was crystallized in the green reduced form at 293 K by mixing 2 µl of a 20 mg ml^{-1} protein solution in 20 m*M* Tris–HCl buffer pH 8 containing 2 m*M* β-mercaptoethanol with 2 µl precipitant solution (3.2 *M* ammonium sulfate in 100 m*M* Tris–HCl buffer pH 8). The drop was equilibrated by vapour diffusion against 1 ml of precipitant solution using a Hampton Research 24-well Linbro plate. Large regular cubic shaped crystals grew to an average size of approximately 0.3 mm after about a week.

2.2. X-ray diffraction data collection and processing

A single crystal of *Rf. fermentans* HiPIP was transferred from the mother liquor to the cryobuffer (20% glycerol and 80% 3.2 *M* ammonium sulfate). After ∼1 min, the crystal was scooped up in a rayon cryoloop and rapidly exposed to a cold nitrogen stream (Oxford Cryosystems Cryostream) on the BW7B wiggler line (λ = 1.105 Å) of the DORIS storage ring at the EMBL Outstation at the Deutsche Elektronen Synchrotron (DESY) in Hamburg (Germany). A 1.45 Å diffraction data set was collected at 100 K using a 30 cm MAR Research imaging-plate scanner (MAR X-Ray Research, GmbH, Hamburg). One crystal was sufficient to complete the data collection. The data set was recorded in two sweeps at different exposure times in order to accurately record both the strongest low-resolution and the weakest high-resolution diffraction intensities. The crystal belonged to space group $P4_32_12$ (the correct enantiomorph was determined at the phasing stage) and the unit-cell parameters were $a = b = 88.31$, $c = 61.34$ Å.

The MAD data set was collected using a different crystal and analogous cryoconditions as described above at EMBL Hamburg beamline BW7A using a 18 cm MAR image plate. Three wavelengths were collected: (i) at the iron-absorption edge (1.742 Å), (ii) near the maximum f'' value on the high-energy side of the edge (1.738 Å) and (iii) away from the edge (0.995 Å). The maximum resolution near the absorption edge was limited to 2.4 Å by the size of the detector. The data set at the third wavelength was collected to 2.1 Å. The unit-cell parameters were $a = b = 88.29$, $c = 61.34$ Å.

Table 2
MAD phasing statistics as a function of resolution (for acentric reflections).

The anomalous $R_{\rm Cullis}$ is defined as the lack of closure divided by the anomalous differences $|F^+ - F^-|$ and the dispersive $R_{\rm Cullis}$ is the lack of closure divided by the dispersive differences $|F(\lambda^i) - F(\lambda^j)|$. The $R_{\rm Cullis}$(anom) is given for anomalous differences at 1.738 Å and the $R_{\rm Cullis}$(energy-dispersive) is given for the dispersive differences between the amplitudes at 0.995 and 1.742 Å.

Resolution (Å)	Figure of merit	$R_{\rm Cullis}$(anom)	$R_{\rm Cullis}$(energy-dispersive)
7.42	0.92	0.31	0.24
4.76	0.83	0.51	0.33
3.76	0.72	0.75	0.44
3.20	0.69	0.83	0.50
2.83	0.66	0.84	0.51
2.57	0.52	0.89	0.55
2.37	0.47	0.88	0.60

All the data (three-wavelength MAD and high-resolution) were integrated with the program *MOSFLM* (Leslie, 1991). The data were scaled and merged with *SCALA* (Collaborative Computational Project, Number 4, 1994). The MAD data sets at all three wavelengths were merged together to provide a reference data set for the local scaling procedure proposed by Evans (1997) to reduce systematic errors in the anomalous and dispersive differences. The structure-factor amplitudes were calculated with the program *TRUNCATE* (Collaborative Computational Project, Number 4, 1994; French & Wilson, 1978). The overall temperature factor was estimated from Wilson plots (Wilson, 1942). Data statistics derived from data processing are shown in Table 1.

2.3. Structure solution

After several unsuccessful attempts to solve the structure by molecular replacement using other known HiPIP structures, MAD phasing was attempted instead. The main difficulty in the MAD approach was to locate the individual Fe atoms in the cubane cluster. The resolution of the data set with the maximum anomalous contribution from iron was not high enough to resolve the individual atoms. The program *SHELXD* (Usón & Sheldrick, 1999) successfully located three clusters in the asymmetric unit. The cluster coordinates were refined and used to calculate MAD phases with *SHARP* (de La Fortelle *et al.*, 1997). Although the first electron-density maps were not clearly interpretable, the dispersive difference logarithmic likelihood maps (de La Fortelle & Bricogne, 1997) calculated with the coefficients from the remote and inflection wavelengths revealed positive peaks at some of the correct Fe-atom positions from which better phases could be obtained. After several cycles of heavy-atom parameter refinement, phasing and inspection of difference logarithmic likelihood maps, all 12 Fe atoms in the asymmetric unit were correctly identified. The final phasing statistics using all Fe atoms are shown in Table 2.

Density modification and phase extension to 1.45 Å were performed with the *CCP*4 program *DM* (Cowtan, 1994). The resultant electron density was of high quality and allowed automated model building using the 'warpNtrace' option in the program *wARP* (Perrakis *et al.*, 1999). The assignment of free water atoms to peaks in the density map was combined with automated tracing by searching the free-atom model for adjacent atoms fulfilling the distance and angle criteria expected for peptide chains, with refinement with the program *REFMAC* (Collaborative Computational Project, 1994) using a maximum-likelihood target (Murshudov *et al.*, 1997). Side chains were assigned using the 'side-chain dock' option of *wARP*. Disordered areas and side chains were built manually. Inspection of the maps and models was performed on an SGI Octane workstation with the program *TURBO-FRODO* (Roussel & Cambillau, 1991).

Table 3
Restraint information.

	No.	R.m.s.d.	σ
Bond distance (Å)	1750	0.008	0.02
Angle distance (Å)	2371	0.026	0.04
Planar 1–4 distance (Å)	632	0.068	0.05
Peptide planes (Å)	223	0.023	0.03
Aromatic planar groups (Å)	21	0.009	0.02
Chiral volumes (Å^3)	260	0.098	0.15
VdW single torsion (Å)	588	0.157	0.30
VdW multiple torsion (Å)	1214	0.259	0.30
Hydrogen bond (Å)	63	0.124	0.30
Planar torsion angles (°)	224	8.40	7.00
Staggered torsion angles (°)	312	13.90	15.00
Orthonormal torsion angles (°)	21	15.80	20.00
NCS positional (Å)	1108	0.411	5.00
NCS thermal (Å^2)	1108	3.440	10.00
B restraint (main-chain bond) (Å^2)	1049	1.311	2.00
B restraint (main-chain angle) (Å^2)	1257	1.908	3.00
B restraint (side-chain bond) (Å^2)	701	1.508	2.00
B restraint (side-chain angle) (Å^2)	1114	2.079	3.00
B sphere (Å^2)	2023	2.607	2.00
Rigid-bond *U* restraint (Å^2)	1750	0.679	1.00

2.4. Refinement and validation

The initial model was refined by the conjugate-direction method (Tronrud, 1992) as implemented in *REFMAC*, with the geometry restrained to the standard Engh and Huber values (Engh & Huber, 1991), using the maximum-likelihood target. The model was refined against the high-resolution data set, but using experimental MAD phases blurred by a scale factor of 0.5 as a restraint. Loose NCS restraints were also applied to most residues in the monomer (except for the two N- and C-terminal residues). The first cycles of refinement with *REFMAC* were combined with automatic water-molecule searching using *ARP* (Lamzin & Wilson, 1997). Many water molecules (~50) were clearly related by the NCS operators and their refinement was also restrained. H atoms were generated before the refinement using a bond length of 1 Å and their contribution to the structure factors was calculated with *SFALL* (Collaborative Computational Project, Number 4, 1994) for use in the refinement.

After refinement, the fit of the model to the electron density was inspected using $2mF_o - DF_c$ and $mF_o - DF_c$ difference Fourier density maps, where F_o and F_c are the scaled observed and calculated structure factors, m is the figure of merit and D is an estimate of the error in the partial structure from co-

Table 4
Summary of the refinement.

	Chain *A*	Chain *B*	Chain *C*
Refined residues	75	74	74
Residues with multiple conformation	8	6	5
Solvent atoms	104	72	100
Fe–S clusters	1	1	1
Sulfates	3	1	1
Ramachandran plot			
Most favoured region (%)	68	69	69
Allowed region (%)	6	4	4
Generously allowed region (%)	1	1	0
Disallowed region (%)	0	0	1
R factor (all reflections)	0.186		
R_{free}	0.218		
Correlation coefficient (all reflections)	0.949		
Correlation coefficient (R_{free} set)	0.926		
Overall coordinate e.s.u.†	0.032		
Overall *B* e.s.u.†	0.839		

† Based on maximum-likelihood target $R = \sum(|F_o| - |F_c|)/\sum|F_o|$.

ordinate errors (Luzzati, 1953). These coefficients were calculated using *REFMAC*.

Both isotropic and anisotropic temperature factors were refined for individual atoms (Murshudov *et al.*, 1999). For the anisotropic refinement, the atomic anisotropic tensor was restrained to prevent large departures from spherical symmetry and to similar values for neighbouring atoms ('rigid-bond' restraint). A list of all restraints, targets and root-mean-square (r.m.s.) deviations of the final model for the refinement is given in Table 3. The results of the refinements and the stereochemical analysis of the model, carried out with *PROCHECK* (Laskowski *et al.*, 1993), are summarized in Table 4.

3. Structure description

3.1. The monomer

The three monomers found in the asymmetric unit feature a pairwise r.m.s.d. of 0.37 Å (the maximum distance between equivalent atoms is 2.5 Å), which indicates an overall high similarity. The protein chain consists of a helix (residues 10–15) and two short 3_{10}-helices (21–23, 38–40), numerous hairpin turns predominantly of type I, as well as a small β-sheet formed by two short antiparallel β-strands (51–52 and 62–63; Fig. 1*a*). The N- and C-terminal segments are largely unstructured, with short stretches of the backbone in β-folding. All residues are in allowed regions of the Ramachandran plot (Table 4), except Lys47 in the turn 46–49 (type I). The main-chain amino N of this residue forms a hydrogen bond to a well ordered structural water molecule (water 19; waters 1019 and 2019 in chains *B* and *C*, respectively), which forces the backbone into a strained conformation ($\varphi = 53$, $\psi = -121^\circ$).

There are several structural waters contributing to the stability of the monomer, such as water 6 (1006 and 2006) in the cavity formed by the turns 9–12 (type I) and 57–60 (type II), water 1 (1001, 2001) surrounded by the conserved aromatic residues enclosing the Fe–S cluster and water 4 (1004, 2004) between the turn 6–9 and the fully conserved residue Tyr17.

The monomer dimensions are approximately 30 × 24 × 14 Å. When viewed perpendicular to the long axis, the monomer resembles a letter W, with the two outer arms formed by the loops comprising residues 49–63 and 21–36 and the $[Fe_4S_4]$ cluster nested under one of the arches (Fig. 1*b*). The tip of the W arms close to the $[Fe_4S_4]$ cluster constitutes a hydrophobic surface, formed by the side chains of residues Leu15, Leu43 and Leu56, which are highly conserved in all HiPIPs (Van Driessche *et al.*, 1997). This surface patch has been proposed to be a key site for molecular-recognition processes mediated by hydrophobic interactions. A possible binding site in the vicinity of the heme 1 site on the tetraheme cytochrome subunit of the photosynthetic RC has been identified on the basis of mutagenesis studies of the RC of *Ru. gelatinosus* (Osyczka, Nagashima, Shimada *et al.*, 1999; Osyczka, Nagashima, Sogabe *et al.*, 1999).

Much of the rest of the *Rf. fermentans* HiPIP surface presents a positive charge because of the abundance of exposed lysines. There are 11 lysines in the monomer. Of these, only three are largely conserved amongst the known HiPIPs: Lys23 and Lys60, which form a bond to the also rather conserved Asp9 and probably contribute to the overall stability of the monomer, and Lys74, at the C-terminal end, which blocks a side of the cavity containing the $[Fe_4S_4]$ cluster and might be involved in electron transfer. Almost half of the lysines in this protein are in surface loops presenting poor sequence and structure alignment with other studied HiPIPs, with the exception of the most closely related *Ru. gelatinosus*.

3.2. Monomer–monomer interactions: trimer and crystalline arrangement

Chains *A* and *B* of the basic trimer are related by a twofold axis almost perpendicular to the crystallographic *c* axis and parallel to the long axis of the monomer, while the chain *C* long axis is at an angle (about 20°) with respect to *A* and *B*. The contacts between monomers and crystallographic symmetry-related units take place predominantly along the *a* and *b* axes. Although the contacts are not symmetrical because of the improper NCS symmetry, the close packing along the *a* and *b* directions does not disturb the folding of the chain, with significant differences between the chains found only at the N- and C-termini. Here, the chains have different levels of exposure to the solvent regions, with the N-terminus of chain *B* and the C-terminus of chain *C* pointing directly into solvent regions and being so disordered that the terminal residues could not be modelled.

There are few direct bonds between the monomers. Many contacts are mediated by water-molecule clusters trapped in the cavities formed by the protein-chain folds. An example of this type of contact is shown in Fig. 2. There are also hydrophobic interactions amongst residues in the conserved hydrophobic patch near the $[Fe_4S_4]$ cluster. Hydrophobic interactions between HiPIP monomers have also been observed in solution (Bertini *et al.*, 1993). The differences in

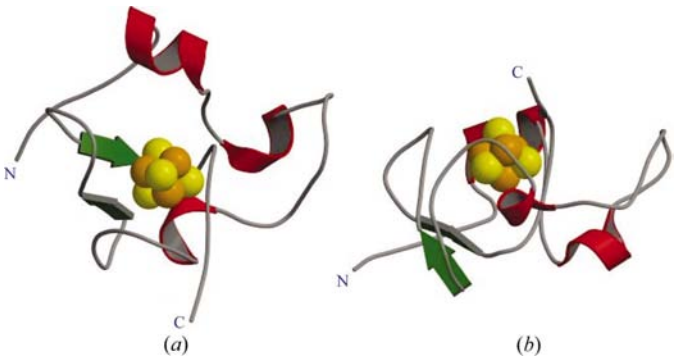

Figure 1
Ribbon schematic views of the *Rf. fermentans* monomer, showing the major secondary-structure elements and the [Fe_4S_4] cluster (Fe, orange; S, yellow). The figures in (*a*) and (*b*) are related by a rotation of 90° around the horizontal axis.

the interactions between the monomers in the crystal subunit of this structures and the wide range of different dimeric structures found amongst other HiPIPs (Kerfeld *et al.*, 1998; Parisini *et al.*, 1999) suggest that the monomer is more likely to be the active form of the protein.

3.3. Crystal solvent

About 48% of the unit cell is occupied by solvent. The Matthews coefficient (Matthews, 1968) is 2.5 $Å^3\ Da^{-1}$. The tightly packed protein monomers along *a* and *b* define a rectangular solvent well about 20 Å wide by 65 Å long. The protein surface exposed to the solvent is highly positively charged, with 27 out of 33 lysine side chains in the basic trimer facing the central well. Another interesting solvent region is a 8 Å radius pocket enclosed by the residues Lys26, Lys31, Thr33 and Lys34 of chains *A* and *B* about the crystallographic *c* axis. The strong positive charge on the surface of the pore attracts the sulfate ions present in the crystallization buffer. These sulfate ions bind to the lysine side chains and are probably important for the stability of the crystalline form. The region of the protein containing the residues involved in these contacts presents little homology with other HiPIP structures, which may explain the different packing in these crystals compared with other known HiPIP crystal structures. Sulfate ions have also been found to bind to *Thermochromatium tepidum* HiPIP, which was also crystallized in the presence of ammonium sulfate (Liu *et al.*, 2002).

3.4. Comparison with HiPIPs from other species

An overall comparison of HIPIPs of different species for which a crystal structure is available shows that despite the relatively low sequence identity (ranging from 26 to 37%), most structures are rather similar (Fig. 3), with typical average differences in the backbone atom positions of about 1 Å. Larger differences are found particularly at two of the surface loops comprising Ala24–His32 and Lys47–Lys49 (Fig. 3). The HiPIPs of the genus *Chromatium* have a large sequence identity in these zones as well as the same structure, with some small differences in the second stretch. The *Rf. fermentans*

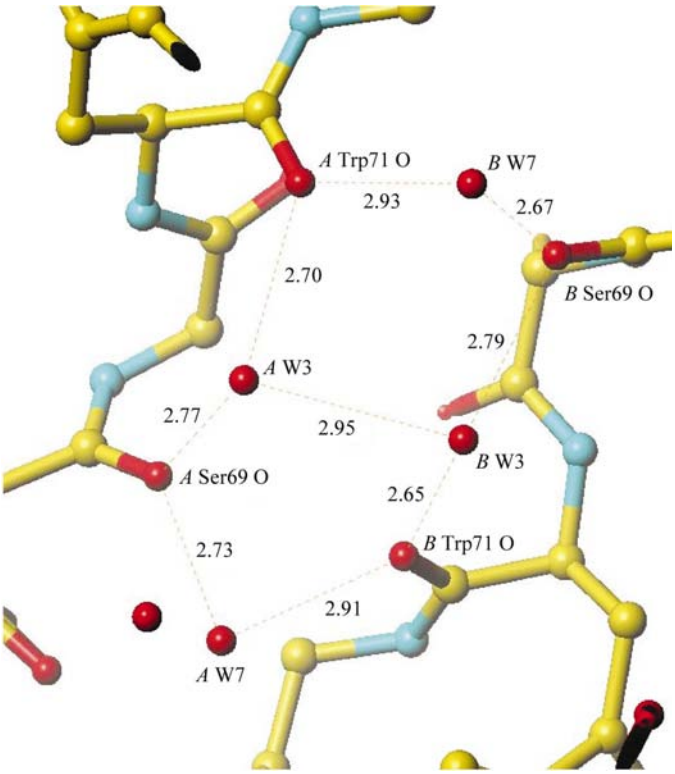

Figure 2
An example of water-mediated contacts is the extended arm of the C-terminal backbone comprising residues 69–73 in chains *A* and *B*. The NCS twofold axis relating these chains runs perpendicular to these residues. Contacts between monomers take place though waters 3 and 7 (and their respective NCS partners in the other chain). Water 7 is hydrogen bonded to Lys73 N and Trp71 O of chain *B* and Ser69 of chain *A*. The hydrogen-bond lengths are given.

HiPIP sequence has some deletions in these zones and practically no sequence identity to other HiPIP crystal structures and not only has shorter loops with fewer turns, but also has a markedly different structure in these zones. Moreover, the *E. halophila* HiPIP lacks the short helix near the N-terminus. *Rc. tenuis* is the HiPIP structure with most differences, with an r.m.s. difference of about 3.2 Å between the main-chain atoms in the sequence-alignment regions (the corresponding differences are 2.5 Å for *T. tepidum* and 1.1 Å for *C. vinosum*).

The HiPIP structures feature the largest degree of similitude around the cavity enclosing the [Fe_4S_4] cluster, involving residues 16–20, 35–45, 55–69 and the C-terminal arm. These stretches contain the four cysteine residues that bind to the S atoms in the cluster (Cys38, Cys41, Cys55 and Cys68; shown in Fig. 4) in addition to the highly conserved residues Tyr17, Tyr44, Phe57 and Trp67, which limit the solvent accessibility to the cluster, thus preventing hydrolysis in the oxidized state. It is not known whether some or all these residues also play a role in electron transfer.

The hydrophobic surface is also structurally similar to the other HiPIP structures, particularly to the *C. vinosum* HiPIP family, although the backbone structure differs in the case of *E. halophila* and differs even more in the case of *Rc. tenuis*. Differences might also occur in the structure of the binding site in the corresponding RCs.

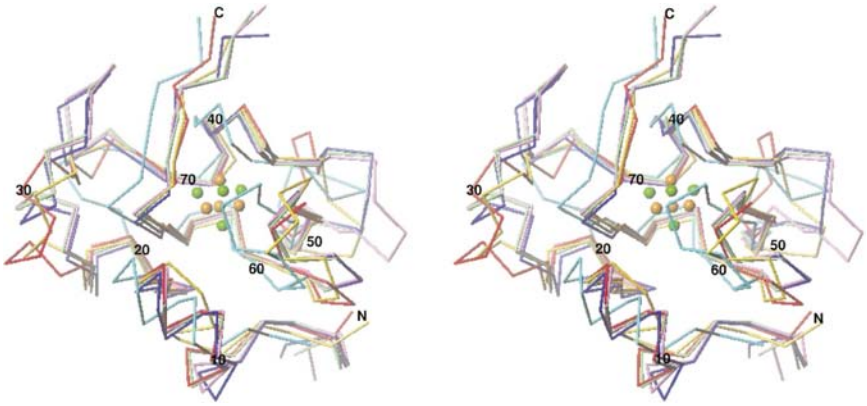

Figure 3
Structure alignment of HiPIP structures. Stereoview of the C^{α} chain of *Rf. fermentans* (red), *C. vinosum* (mauve, 35% sequence identity), *T. tepidum* (dark blue, 33%) and *C. purpuratum* (green, 28%), *E. halophila* (yellow, 37%) and *Rc. tenuis* (light blue, 26%). The $[Fe_4S_4]$ cluster for *Rf. fermentans* is also shown. The residue numbers shown are for the *Rf. fermentans* model. The structure alignment matches the sequence alignment given by Van Driessche *et al.* (1997).

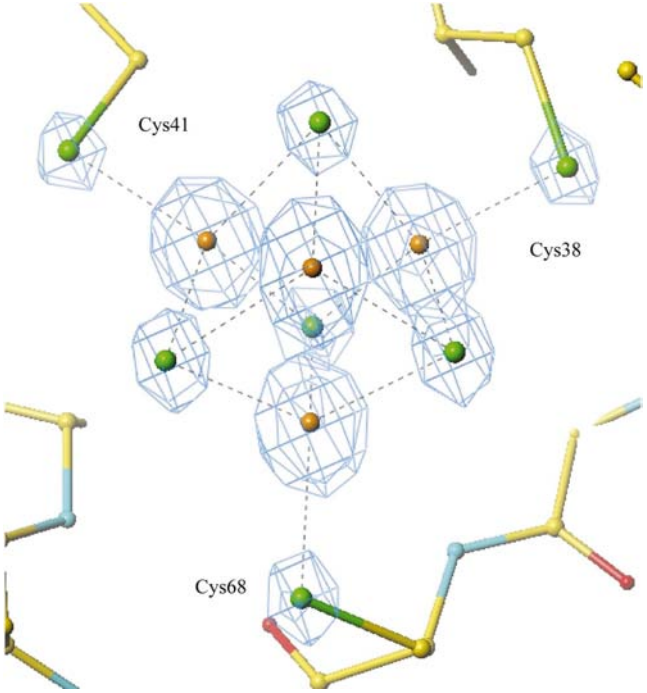

Figure 4
View of the cubane molecule showing the bonds to Cys38, Cys41 and Cys68 (the bond to Cys55 is perpendicular to the plane of the picture and is not shown). The Fe—S bond lengths are between 2.24 and 2.34 Å. The electron-density map is contoured at 8σ.

4. Summary

MAD methods were successfully applied to determine the structure of the *Rf. fermentans* HiPIP. The structure solution illustrates a potential problem using heavy-atom clusters (for example, TaBr or W clusters) to phase macromolecules. If the individual atoms in the cluster cannot be resolved to their correct position, the quality of the maps will be greatly reduced. In the case presented here, having a single iron site incorrectly assigned (of the 12 in the asymmetric unit) made the maps non-interpretable. Having good enough data resolution to locate the sites in difference Fourier maps after phasing was crucial to the success of phasing. Model building and refinement was straightforward, except for some disordered stretches at the N- and C-termini of the chain.

The protein monomer is folded tightly into numerous loops. Although three monomers were found in the asymmetric unit, there is no evidence that the trimer corresponds to the organization of the active molecule *in vivo*. It is more likely to be an artefact of the crystal packing. A distinctive feature of the protein is a large positively charged surface. While there is some evidence for a role of net surface charges in the HiPIP–RC interaction (Hochkoeppler *et al.*, 1996), the role of most of the numerous lysines present in this particular case remains unknown.

The structure presents a large degree of structural homology with other HiPIP structures in the protein core surrounding the cubane molecule. The largest differences between HiPIPs are observed in external loops that correspond to insertion or deletion areas in the sequence alignment. The *Rf. fermentans* HiPIP is most closely related to the HiPIP from *Ru. gelatinosus* based on the sequence similarity (57%, compared with no more than 37% for other HiPIPs). The structure of the *Rf. fermentans* HiPIP is the only one determined for its subclass so far. It is therefore a basic representative of other HiPIPs of another group and is potentially a useful model for post-genomics and structural genomics studies.

References

Aprahamian, G. & Feinberg, B. A. (1981). *Biochemistry*, **20**, 915–919.
Babini, E., Bertini, I., Borsari, M., Capozzi, F., Luchinat, C., Zhang, X., Moura, G. L. C., Kurnikov, I. V., Beratan, D. N., Ponce, A., Di Bilio, A. J., Winkler, J. R. & Gray, H. B. (2000). *J. Am. Chem. Soc.* **122**, 4532–4533.
Bartsch, R. G. (1991). *Biochim. Biophys. Acta*, **1058**, 28–30.
Benning, M. M., Meyer, T. E., Rayment, I. & Holden, H. M. (1994). *Biochemistry*, **33**, 2476–2483.
Bertini, I., Ciurli, S. & Luchinat, C. (1995). *Struct. Bonding*, **83**, 1–53.
Bertini, I., Gaudemer, A., Luchinat, C. & Piccioli, M. (1993). *Biochemistry*, **32**, 12887–12893.
Bonora, P., Principi, I., Ciurli, S., Zannoni, D. & Hochkoeppler, A. (1999). *Biochim. Biophys. Acta*, **1410**, 51–60.
Bowyer, J. R., Tierney, G. V. & Crofts, A. R. (1979). *FEBS Lett.* **101**, 207–212.
Breiter, D. R., Meyer, T. E., Rayment, I. & Holden, H. M. (1991). *J. Biol. Chem.* **266**, 18660–18667.
Capozzi, F., Ciurli, S. & Luchinat, C. (1998). *Struct. Bonding*, **90**, 127–160.
Carter, C. W. Jr (2001). *Handbook of Metalloproteins*, edited by A. Messerschmidt, R. Huber, K. Wieghardt & T. Poulos, pp. 602–609. Chichester: John Wiley.
Carter, C. W., Kraut, J., Freer, S. T., Alden, R. A., Sieker, L. C., Adman, E. & Jensen, L. H. (1972). *Proc. Natl. Acad. Sci. USA.* **69**, 3526–3529.

Carter, C. W. Jr, Kraut, J., Freer, S. T., Nguyen-Huu-Xuong, Alden, R. A. & Bartsch, R. G. (1974). *J. Biol. Chem.* **249**, 4212–4225.
Ciurli, S., Cremonini, M. A., Kofod, P. & Luchinat, C. (1996). *Eur. J. Biochem.* **236**, 405–411.
Collaborative Computational Project, Number 4 (1994). *Acta Cryst.* D**50**, 760–763.
Cowtan, K. (1994). *Jnt CCP4/ESF–EACBM Newsl. Protein Crystallogr.* **31**, 34–38.
Dutton, P. L. & Leigh, J. S. (1975). *Biochim. Biophys. Acta*, **314**, 178–190.
Engh, R. A. & Huber, R. (1991). *Acta Cryst.* A**47**, 392–400.
Evans, P. R. (1997). *Proceedings of the CCP4 Study Weekend. Recent Advances in Phasing*, edited by K. S. Wilson, G. Davies, A. W. Ashton & S. Bailey, pp. 97–102. Warrington: Daresbury Laboratory.
Freer, S. T., Alden, R. A., Carter, C. W., Jr., & Kraut, J. (1975). *J. Biol. Chem.* **250**, 46–54.
French, G. S. & Wilson, K. S. (1978). *Acta Cryst.* A**34**, 517–524.
Fukumori, Y. & Yamanaka, T. (1979). *Curr. Microbiol.* **3**, 117–120.
Hiraishi, A., Hoshino, Y. & Satoh, T. (1991). *Arch. Microbiol.* **155**, 330–336.
Hochkoeppler, A., Ciurli, S., Venturoli, G. & Zannoni, D. (1995). *FEBS Lett.* **357**, 70–74.
Hochkoeppler, A., Kofod, P., Ferro, G. & Ciurli, S. (1995). *Arch. Biochem. Biophys.* **322**, 313–318.
Hochkoeppler, A., Moschettini, G. & Zannoni, D. (1995). *Biochim. Biophys. Acta*, **1229**, 73–80.
Hochkoeppler, A., Zannoni, D., Ciurli, S., Meyer, T. E., Cusanovich, M. A. & Tollin, G. (1996). *Proc. Natl Acad. Sci. USA*, **93**, 6998–7002.
Hochkoeppler, A., Zannoni, D. & Venturoli, G. (1995). *Biochim. Biophys. Acta*, **1229**, 81–88.
Hooper, A. B. & Di Spirito, A. A. (1985). *Microbiol. Rev.* **49**, 140–157.
Kerfeld, C. A., Salmeen, A. E. & Yeates, T. O. (1998). *Biochemistry*, **37**, 13911–13917.
Knaff, D. B., Willie, A., Long, J. E., Kriauciunas, A., Durham, B. & Millett, F. (1991). *Biochemistry*, **30**, 1303–1310.
Kusano, T., Takeshima, T., Sugawara, K., Inoue, C., Shiratori, T., Yano, T., Fukumori, Y. & Yamanaka, T. (1992). *J. Biol. Chem.* **267**, 11242–11247.
La Fortelle, E. de & Bricogne, G. (1997). *Methods Enzymol.* **276**, 472–494.
La Fortelle, E. de, Irwin, J. J. & Bricogne, G. (1997). In *Crystallographic Computing 7*, edited by P. Bourne & K. Watenpaugh. Oxford: IUCr/Oxford University Press.
Lamzin, V. S. & Wilson, K. S. (1997). *Methods Enzymol.* **277**, 269–305.
Laskowski, R. A., MacArthur, M. W., Moss, D. S. & Thornton, J. M. (1993). *J. Appl. Cryst.* **26**, 283–291.
Leslie, A. G. W. (1991). *Crystallographic Computing V*, edited by D. Moras, A. D. Podjarny & J. C. Thierry, pp. 27–38. Oxford University Press.
Lin, X., Williams, J. C., Allen, J. P. & Mathis, P. (1994). *Biochemistry*, **33**, 13517–13523.
Liu, L., Nogi, T., Kobayashi, M., Nozawa, T. & Miki, K. (2002). *Acta Cryst.* D**58**, 1085–1091.
Luzzati, V. (1953). *Acta Cryst.* **6**, 142–152.
Matthews, B. W. (1968). *J. Mol. Biol.* **33**, 491–497.
Menin, L., Gaillard, J., Parot, P., Schoepp, B., Nitschke, W. & Vermeglio, A. (1998). *Photosynth. Res.* **55**, 343–348.
Menin, L., Schoepp, B., Parot, P. & Vermeglio, A. (1997). *Biochemistry*, **36**, 12183–12188.
Meyer, T. E., Bartsch, R. G., Cusanovich, M. A. & Tollin, G. (1993). *Biochemistry*, **32**, 4719–4726.
Meyer, T. E. & Donohue, T. J. (1995). *Anoxygenic Photosynthetic Bacteria*, edited by R. E. Blankenship, M. T. Madigan & C. E. Bauer, pp. 725–745. Dordrecht: Kluwer Academic Publishers.
Meyer, T. E., Przysiecki, C. T., Watkins, J. A., Bhattacharyya, A., Simondsen, R. P., Cusanovich, M. A. & Tollin, G. (1983). *Proc. Natl Acad. Sci. USA*, **80**, 6740–6744.
Middleton, P., Dickson, D. P. E., Johnson, C. E. & Rush, J. D. (1980). *Eur. J. Biochem.* **104**, 289–296.
Mizrahi, I. A. & Cusanovich, M. A. (1980). *Biochemistry*, **19**, 4733–4737.
Mizrahi, I. A., Meyer, T. E. & Cusanovich, M. A. (1980). *Biochemistry*, **19**, 4727–4732.
Mizrahi, I. A., Wood, F. E. & Cusanovich, M. A. (1976). *Biochemistry*, **15**, 343–348.
Moser, C. C. & Dutton, P. L. (1988). *Biochemistry*, **27**, 2450–2461.
Murshudov, G. N., Lebedev, A., Vagin, A. A., Wilson, K. S. & Dodson, E. J. (1999). *Acta Cryst.* D**55**, 247–255.
Murshudov, G. N., Vagin, A. A. & Dodson, E. J. (1997). *Acta Cryst.* D**53**, 240–255.
Nogi, T., Fathir, I., Kobayashi, M., Nozawa, T. & Miki, K. (2000). *Proc. Natl Acad. Sci. USA*, **97**, 13561–13566.
Okamura, M. Y. & Feher, G. (1983). *Biophys. J.* **41**, 122a.
Osyczca, A., Nagashima, K. V., Shimada, K. & Matsuura, K. (1999). *Biochemistry*, **38**, 2861–2865.
Osyczca, A., Nagashima, K. V., Sogabe, S., Miki, K., Shimada, K. & Matsuura, K. (1999). *Biochemistry*, **38**, 15779–15790.
Osyczka, A., Nagashima, K. V. P., Sogabe, S., Miki, K., Yoshida, M., Shimada, K. & Matsuura, K. (1998). *Biochemistry*, **37**, 11732–11744.
Osyczka, A., Yoshida, M., Nagashima, K. V. P., Shimada, K. & Matsuura, K. (1997). *Biochim. Biophys. Acta*, **1321**, 93–99.
Overfield, R. E., Wraight, C. A. & De Vault, D. (1979). *FEBS Lett.* **105**, 137–142.
Parisini, E., Capozzi, F., Lubini, P., Lamzin, V., Luchinat, C. & Sheldrick, G. M. (1999). *Acta Cryst.* D**55**, 1773–1784.
Perrakis, A., Morris, R. & Lamzin, V. S. (1999). *Nature Struct. Biol.* **6**, 458–463.
Prince, R. C., Bashford, C. L., Takamiya, K., van der Berg, W. H. & Dutton, P. L. (1978). *J. Biol. Chem.* **253**, 4137–4142.
Prince, R. C., Cogdell, R. J. & Crofts, A. R. (1974). *Biochim. Biophys. Acta*, **347**, 1–13.
Przysiecki, C. T., Meyer, T. E. & Cusanovich, M. A. (1985). *Biochemistry*, **24**, 2542–2549.
Rawlings, J., Wherland, S. & Gray, H. B. (1976). *J. Am. Chem. Soc.* **98**, 2177–2180.
Rayment, I., Wesenberg, G., Meyer, T. E., Cusanovich, M. A. & Holden, H. M. (1992). *J. Mol. Biol.* **228**, 672–686.
Roussel, A. & Cambillau, C. (1991). *Silicon Graphics Geometry Partners Directory 86.* Silicon Graphics, Mountain View, CA, USA.
Schoepp, B., Parot, P., Menin, L., Gaillard, J., Richaud, P. & Vermeglio, A. (1995). *Biochemistry*, **34**, 11736–11742.
Shill, D. A. & Wood, P. M. (1984). *Biochim. Biophys. Acta*, **764**, 1–7.
Tedro, S. M., Meyer, T. E. & Kamen, M. D. (1977). *J. Biol. Chem.* **252**, 7826–7833.
Tiede, D. M., Vashishta, A.-C. & Gunner, M. R. (1993). *Biochemistry*, **32**, 4515–4531.
Tronrud, D. E. (1992). *Acta Cryst.* A**48**, 912–916.
Usón, I. & Sheldrick, G. M. (1999). *Curr. Opin. Struct. Biol.* **9**, 643–648.
Van Driessche, G., Ciurli, S., Hochkoeppler, A. & van Beeumen, J. J. (1997). *Eur. J. Biochem.* **244**, 371–377.
Venturoli, G., Mallardi, A. & Mathis, P. (1993). *Biochemistry*, **32**, 13245–13253.
Wilson, A. J. C. (1942). *Nature (London)*, **150**, 151–152.